Modelling and Characterization of an Integrated Permittivity Sensor

Joshua Bhojwani - s1737171
joshuabhojwani@student.utwente.nl
Electrical Engineering, IDS Group, University of Twente
Supervisor : Dr.Ir. R.J. Wiegerink

***Abstract*—A model of an integrated microfluidic device was fabricated in the MESA+ cleanroom of University of Twente. This device contains several sensors embedded in it, one of them being the relative permittivity sensor. The sensor's behaviour can be understood by performing simulations of it. An optimized design was proposed from the simulation results. After performing the simulations, the behaviour of the sensor was verified. The results of the measurements shows that the sensor did not perform as predicted by the simulations thus several suggestions are presented.**

I. INTRODUCTION

The relative permittivity of a material is a unique property which arises when the substance is subjected to an external electric field. A sensor based on such property can be exploited for different application. For example, being able to detect the relative permittivity in a blood sample allows the user to detect glucose concentrations[1]. Other applications include detecting composition and concentrations of medicine in an infusion pump or intravenous drip and measuring energy content of fuel sources[3].

A team of researchers in the University of Twente[2,3,4] fabricated a microdevice that integrates different sensors as shown in Figure 1. This device allows real-time measurements of fluids while they are flowing through the system. There are two types of relative permivitty sensors found in this device. The first type had been characterized and measurements were obtained. The second type was fabricated, however, it has not been fully characterized yet[3].

In the scope of this paper, the permittivity sensor described above is the subject of investigation. Relevant theories were researched upon, which are then used for the basis of several models for the simulations. Several sensor parameters are altered to see the behaviour of the system. After a proper simulation model is established, the device is tested using different fluids available. The data are then graphed and the results are discussed.

II. THEORY AND DESIGN

A. Permittivity

When a substance is exposed to an external electric field, it will be polarized and creates an electric field that counters the external field. The higher the magnitude of the permittivity, the easier it is to polarize the given substance. The relative

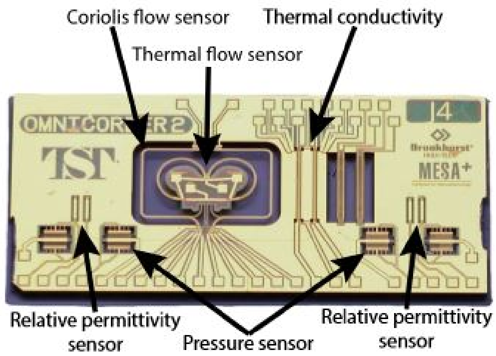

Fig. 1. The sensor chip with the corresponding labels [2]

permittivity (denoted by ϵ_r) is the ratio between the permittivity of the substance and vacuum permittivity (denoted by ϵ_0) and is also known as the dielectric constant [5]. The relative permittivity of a substance can be extracted by measuring the capacitance between two electrodes placed on either side of that substance. Instantaneous polarization increases the capacitance between the two electrodes.

Permittivity varies with frequency and temperatures, however the values can be treated as constants when the substance is tested under low frequencies and steady state. Relative permittivity has a complex numerical value, with real part representing the dielectric constant of the substance and the imaginary part representing the loss factor. The loss factor exists due to the dielectric absorbing the external electric field since work is required to displace the charges. This imaginary part can be assumed negligible when the dielectric is subjected under low frequencies but it is noticeable in the gigahertz frequency range [6].

B. Polarization

There are three kinds of polarization that can occur in a fluid that is exposed to an external electric field. The first one is known as electron polarization. For this type, the electrons are displaced from their usual position, creating a temporary dipole moment; it has the largest contribution to the value of the output from the sensor. The second type is the atomic polarization which is because of the relative change in the average position of the nuclei within the material — the effect of this type is small. The third type is the orientation polarization that causes the molecules to align in the direction of the external field, however its existence is only found in molecules with permanent dipoles such as water, ethanol or glycerol. Because of this third type of polarization, weakly polar liquids tend to have lower ϵ_r compared to strongly polar liquids. Additionally, temperature affects this polarization, as it can influence the strength of the dipole-dipole bond [7].

C. Model designs

The sensor was imaged under the SEM and depicted in Figure 2. For simplifying the simulations, the width of the channel is wide enough to approximate it as parallel plate capacitors. Based on Figure 2, a 2D cross-sectional design can be extracted and is shown in Figure 3 which will be utilized for the simulations later on. This figure also showed the dimensions extracted from the SEM . In this diagram, C1 represents the capacitance between the two comb electrodes deposited on the top of the roof, while C2 represents the capacitance between the positive terminal and the lower end of the silicon-rich silicon nitride layer (denoted by Si_xN_y) and C3 represents the capacitance between the negative terminal and the lower end of the Si_xN_y layer.

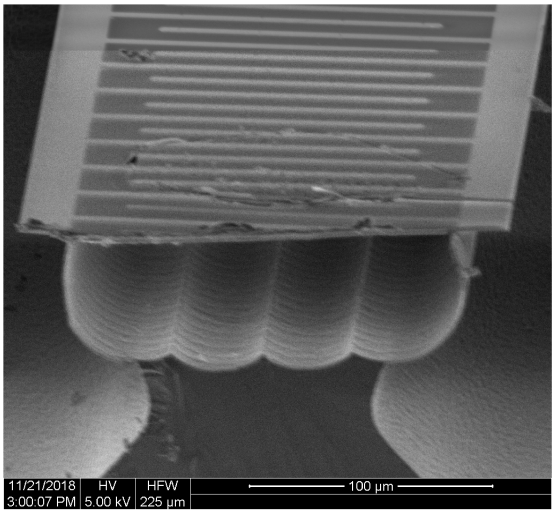

Fig. 2. SEM image of the cross sectional view of the relative permittivity sensor

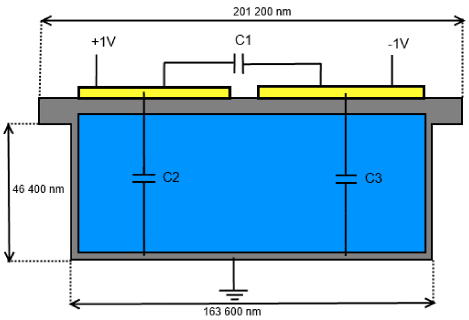

Fig. 3. 2D cross-sectional design of the sensor. Blue represents the dielectric fluid, grey represents the silicon nitride layer and yellow represents the interdigitated capacitors

D. Relevant equations

Equations used for confirming the simulations include:

a) Faraday's capacitor equation[8]:

$$C = \frac{q}{V} \tag{1}$$

where q represents the charge of the capacitor and V represents the voltage across the capacitor.

b) Parallel plate capacitance[9]:

$$C_{parallel} = \frac{\epsilon_r \times \epsilon_0 \times A}{d} \tag{2}$$

where d is the separation between the plates, ϵ_r is the relative permittivity, ϵ_0 is the permittivity of free space (ϵ_0 = 8.854 $\times$ 10^{-12} Fm^{-1}) and A is the area of one of the plates.

c) Interdigitated capacitor[9]:

$$C_{comb} = \frac{\epsilon_r \times \epsilon_0 \times l_0 \times (n-1) \times t}{d} \tag{3}$$

where n is the number of fingers in each comb, l_0 is the common length of the fingers and t is the thickness of the fingers. The rest of the symbol has the same representation as that of equation (2). This equation serves only as an approximation since the effect of fringe fields are ignored. The total capacitance in an interdigitated finger is more complicated than this.

III. Simulations

The simulations were conducted using the Comsol Multiphysics 5.3a simulation software [10] which uses the finite elements method for its calculations. The physics chosen for this process was the Electrostatics physics under the AC/DC module. There were two models that were developed. The first model was designed without the interdigitated fingers on top of the roof. This model served as a method to check the conformity of the simulations with that of theory as a control system. After this model had been validated, a second model was designed by adding the interdigitated fingers on top of the Si_xN_y roof and utilizing the proper parameters. During the simulations, ϵ_r was assumed to be 9.7 for the Si_xN_y layer [11]. Finally, several sensor parameters such as finger length and finger spacing were varied for optimization purposes. Table I lists down all the dimensions that were used during the simulations. The values are fixed unless stated in the following paragraphs.

A. First design

The first design contained the Si_xN_y roof which acts as the electrode and the channel walls. The width of the channel is smaller than the width of the roof, which is displayed in Figure 3. The cross-sectional dimensions were also taken from this figure. This design is extruded to 1 mm. For the analytical calculations, equation (1) is used. For simplicity of calculations, the top and bottom plates are regarded of the same width. Figure 4 displays the calculation results. Simulation 1 infers that the chip is an isolated environment while in simulation 2 the chip is subjected to air, making simulation 2 closer to reality. The values computed in simulation 1 is similar with that of the analytical calculations, especially when dealing with materials with low ϵ_r. Hence it is justified to proceed to the second design.

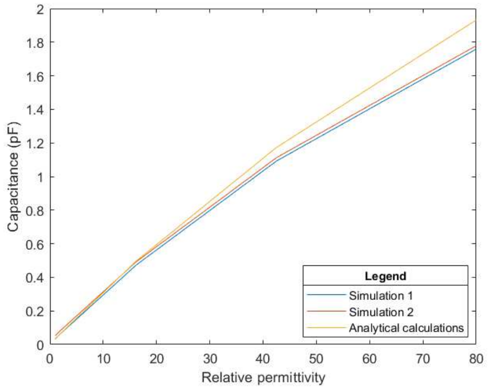

Fig. 4. Graphical representation of all the calculations performed for the first design

TABLE I
SENSOR DIMENSIONS USED THROUGHOUT THE SIMULATIONS

Variable	Value (μm)
roof width	201.2
roof thickness	3
channel width	106.8
channel thickness	1
channel height	46.4
finger separation	10
finger thickness	3
finger length	137.5
system length (1st design)	1000
system length (2nd design)	2000
thickness of gold layer	0.2

B. Second design

For the second design, the chip is extruded to 2 mm and interdigitated fingers are added on top of the channel roof. The fingers are made of gold with a thickness of 200 nm. The dimensions used for this stage are listed in Table I. Throughout this second design, all the values are fixed except for the finger length and the finger separation. These alterations are done in the later stages.

The design is then simulated with material sweep twice — one simulation with the bottom electrode grounded and one with the bottom electrode floating. The positive terminal is set to +1.0 V and the negative terminal is set to -1.0 V as presented in Figure 3. The number of fingers used for this simulation is 238. The program automatically calculates the total capacitance and the result is shown in Figure 5. From this figure, it is evident that the values from the grounded simulations are only higher by a negligible margin than the ones from floating simulations, implying that the sensor output does not depend on grounding of the chip. This is in agreement with what was mentioned by the literature about this sensor [3].

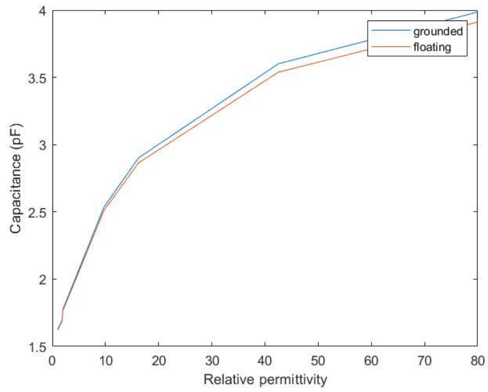

Fig. 5. The capacitance measured with and without grounding

A problem that users of Comsol will face when creating such complex systems is that the program does not show how it calculates the capacitance. When using Comsol's automatic calculation of the capacitance while varying the number of fingers, graphs such as in Figure 6 is produced. This result is not reliable as there can be two values of ϵ_r for each value of capacitance.

The setup that will be used during the measurements is presented in Figure 12. In this setup, one of the terminals of the sensor is connected to a gain-phase analyzer and the other to the charge amplifier. Further details about this setup is covered in the next section. During the measurements ideally only C1 is needed, therefore two methods are presented for tackling this problem.

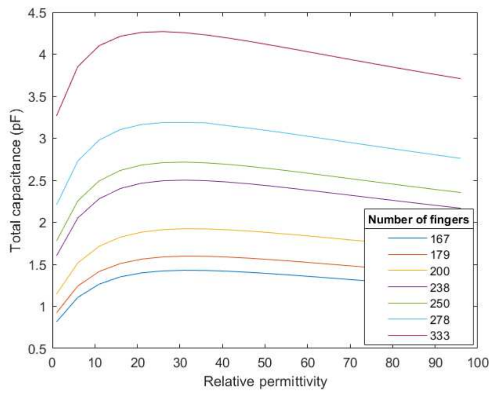

Fig. 6. Total capacitance estimated by Comsol

For the first method, two simulations are needed. In the first simulation, the left terminal is fed with +1.0 V and the right terminal is grounded, rendering C3 inactive. The total capacitance at this stage is C1+C2. In the second simulation, both terminals are fed with +1.0 V. This forces the voltage across C1 to be 0.0 V. The total capacitance now is C2+C3. Thus C1 can easily be calculated analytically. In both simulations a parametric sweep of ϵ_r with step size of 5 is applied. The separation between the fingers is reduced to allow more room for additional fingers to the design. The result of this method is shown in Figure 7.

For the second method, only one simulation is necessary. The positive left is fed with +1.0 V and the right terminal with +0.5 V. Comsol generated two values of charges, which correspond to the charges at the nodes. C1 is yielded by finding the charge difference and utilizing equation (1) and the resulting graph is shown in Figure 8. This figure also displays the difference between the two methods for 167 fingers. This difference is negligible thus both methods are analogous.

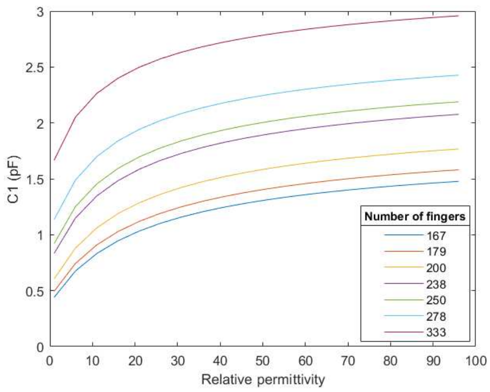

Fig. 7. Determining C1 with the 1st method

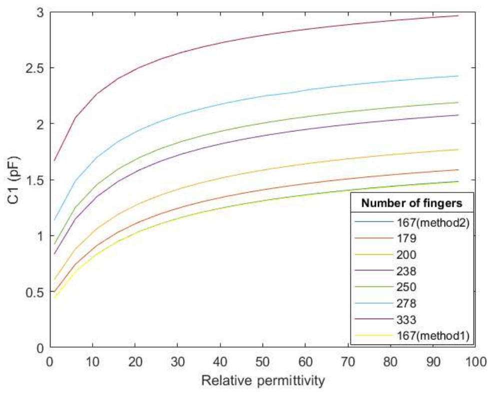

Fig. 8. Determining C1 with the 2nd method

Futhermore, the sensor dimensions are varied. From the previous data, the relationship between C1 and the number of fingers as well as finger spacing can be easily found as seen in Figure 9 and Figure 10 respectively. Figure 9 displays a linear relationship which matches with the expectation based on equation (3). Figure 10 shows an inverse relationship, which is also expected by equation (3).

Then the finger length is modified. For this simulation, 278 fingers and ϵ_r of 5 are chosen. The finger length is modified in the range of 82.5-157.5 μm with steps of 5 μm. This is presented in Figure 11. Equation (3) estimates that the capacitance will increase linearly with respect to the finger length and that is confirmed with what is observed in Figure 11.

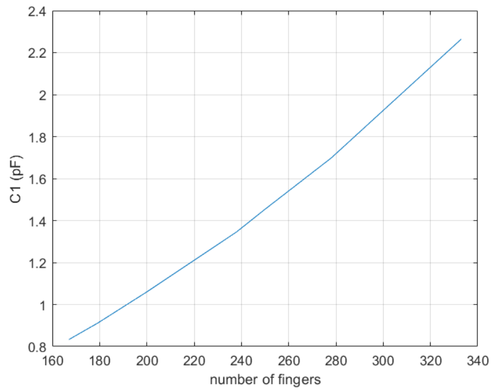

Fig. 9. Capacitance vs number of fingers for ϵ_r = 11

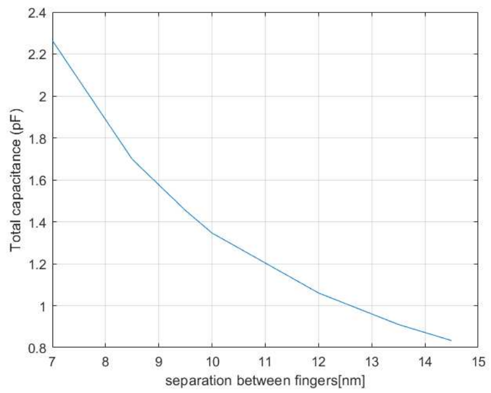

Fig. 10. Capacitance vs separation of fingers for ϵ_r = 11

IV. Experimental procedure and results

The circuit diagram for the measurement set up is shown in Figure 12. From this figure, Cf and the operational amplifier constitute the charge amplifier. A charge amplifier converts charge to voltage, and it has a stated capacitance of 4.7 pF. The system is connected to output and input of HP 4914A gain phase analyzer, which has several modes available for data gathering. Throughout the experiments, the mode chosen is the gain-phase mode, which produce the output in a logarithmic

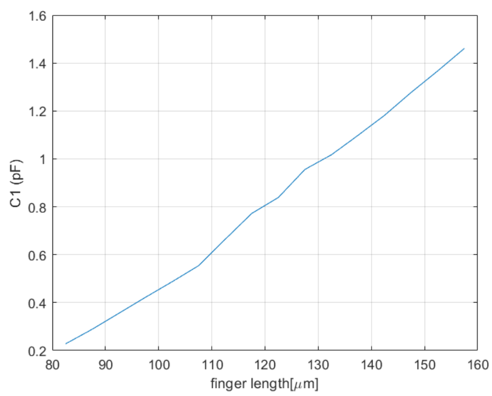

Fig. 11. Capacitance vs finger length for ϵ_r = 5

scale with the base of 10. One of the output of the gain phase analyzer is connected to the reference input since it functions as a reference. Cx denotes the sensor which comprises of C1, C2 and C3.

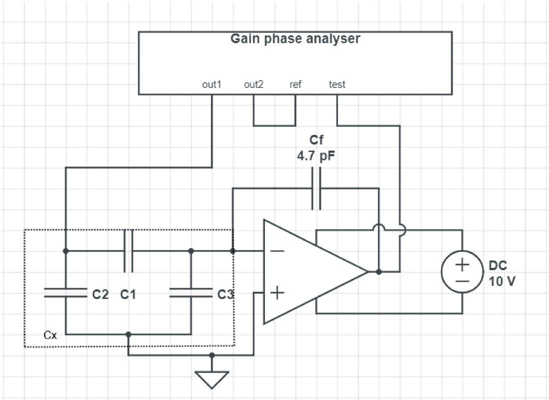

Fig. 12. A measurement setup for the experiments

Before measuring directly with the sensor, calibration of the setup is required. One method of performing the calibration is to have capacitors with known values taking the role of Cx and do calculations with them by assuming that Cf is not known. A frequency sweep between 100 Hz and 1 MHz is done and the result is shown in Figure 13. The peaks that are visible in the lower frequency ranges (below 200 kHz) are due to the frequency response of the charge amplifier. In that figure, it is clear that the response is flatter when using capacitance of values lower than 10 pF. The gains at the flat regions were used for calculating the Cf values and Table II displays this result. This table proofs that the setup is not suitable for high capacitance values since the output values are not in the order of magnitude as the original value of Cf. On the other hand, the simulations shows the expected values for the output to be below 5 pF.

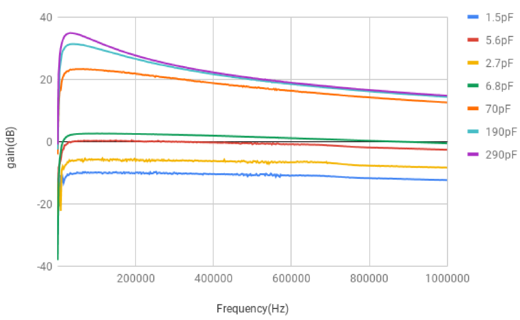

Fig. 13. Gain versus frequency for known capacitance values

Afterwards, the sensor needs to be tested. The fluids that are used are listed in Table III [12]. A frequency sweep of 100 Hz until 1 MHz is used and Figure 14 is generated. The data from the linear regions are extracted to calculate the Cx values according to this setup. From those values, a plot of Cx against ϵ_r is created and is displayed in Figure 15.

TABLE II
CF VALUES ACCORDING TO THE EXPERIMENT RESULTS

Cx(pF)	gain(dB)	Cf(pF)
1.5	-10.905	5.264
2.7	-6.598	5.763
5.6	-0.843	6.200
6.8	1.104	5.988
70	16.324	10.628
190	18.386	22.88
290	18.881	32.987

TABLE III
FLUIDS USED DURING THE EXPERIMENTS

Fluid	ϵ_r
Water	80
Methanol	33.1
Ethanol	24.3
Isopropanol	18
air	33.1

V. DISCUSSION

The entirety of this project deals with the modelling and the characterization of the device. The modelling part concerns with the models that were developed in Comsol Multiphysics 5.3a and the results that emerged from those. A suitable circuit diagram was designed prior to the development of the 3D model. Firstly, a model without the interdigitated fingers was constructed and this model performed as expected. Next, the interdigitated fingers were placed on top of the channel roof and the terminals were assigned accordingly. There were two methods presented which can extract the value of C1 solely. The method that exploits charges has an advantage over the other because it consumes lesser time. Future designers are advised to proceed using the charge method.

For future designers, it is important to note that the readout depends on how deep the electric fields can penetrate into the fluid. In the case of Figure 8, as the number of fingers are increased, the capacitance change with respect to the relative permittivity reduces. When the separation between the fingers are reduced, most of the electric field lines extend from one terminal to the other. Thus, the electric field cannot penetrate deeply into the fluid, causing the readout to be heavily dependent on the interdigitated capacitor. Increasing the separation will allow the electric field to permeate deeper

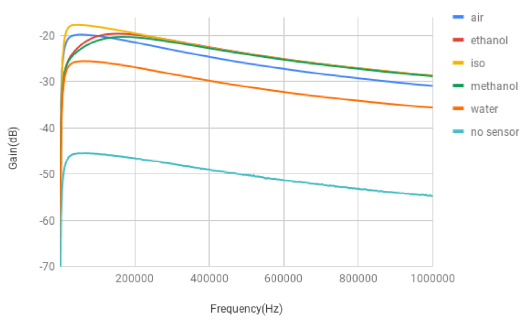

Fig. 14. Gain versus frequency of the sensor

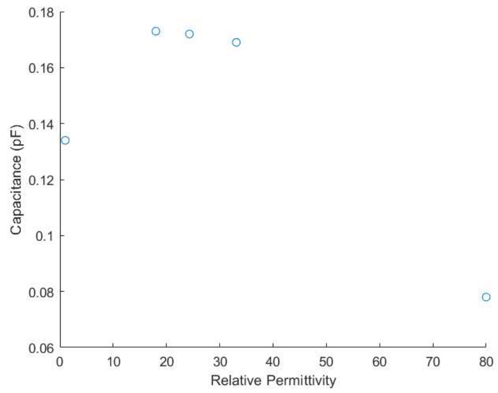

Fig. 15. Cx versus permittivity obtained from the experiments

into the fluid and the capacitance will reduce. If the device used for the readout is not precise enough, those values will be too small to be detected. The same goes with the finger length. The longer the fingers, the lesser the field can penetrate into the fluid. On the contrary, the shorter the fingers, the more the field can penetrate the fluid with the trade off of small readout values.

The characterization part of this project concerns the performance of the device under test. Before doing the measurements with the sensor, a calibration method was outlined and confirmed. This setup was shown to be suitable for low capacitance values. The chosen frequency sweep is such that the loss factor discussed earlier would not affect the measurements. The frequency response of the charge amplifier is dominant in frequencies lower than 200 KHz as seen in Figures 13 and 14. There were several unforeseen outcomes that arose. The capacitance values observed in Figure 15 were smaller than anticipated and the behaviour resembles that of Figure 6 instead of Figure 8. This implies that the output signal is not dependant on C1 only but it measures the total capacitance instead. Contradictory to the theory, the value of the capacitance using water is measured to be lower than that of air. The trend goes down after isopropanol was tested, while Figure 6 predicts that it will decrease gradually when ϵ_r is above 30. A possible reason for the decreasing capacitance for large ϵ_r is due to the increasing capacitance to the grounded silicon substrate. To have a comprehensive idea of the trend, the sensor should be tested with other fluids that have ϵ_r between 30 and 80. Examples of such fluids are - glycerol (ϵ_r = 42.5), acetamide (ϵ_r = 59.2) and ethylene glycol (ϵ_r = 37) [12].

VI. Conclusions

The objective of this project is to propose a model of a fabricated integrated ϵ_r and characterize it. Based on the image drawn out from an SEM, a 2D was made which was then translated into a 3D model. The software Comsol Multiphysics 5.3a was utilized. This model was tested and two methods were proposed to extract the desired quantity, C1, to be measured. The model operated as desired.

The sensor was characterized using the proposed setup consisting of a charge amplifier, gain-phase analyzer, a DC voltage source and the sensor itself. A method for calibration was then devised which required general capacitors. From that result, it is clear that the frequency response of the charge amplifier played a role in low frequency values. Afterwards, measurements with the sensor were conducted. The results were not promising as it deviates from the expectation by a large margin. Therefore, further studies will need to be done. The device was prone to breaking quite easily. A method to solely extract the value of C1 during the experimental process will need be considered. Additionally, the device should be tested with other fluids to grasp the full behaviour it.

References

[1] X.Huang et al. A microfabricated dielectric sensor for continuous glucose monitoring.

[2] J. Groenestijn, M.J. de Boer, J.C. Lotters and R.J. Wiegerink. A versatile technology platform for microfluidic handling systems part 2: channel design and technology. *Microfluid Nanofluid (2017) 21:126*

[3] J. Groenestijn et al. FULLY INTEGRATED MICROFLUIDIC MEASUREMENT SYSTEM FOR REAL-TIME DETERMINATION OF GAS AND LIQUID MIXTURES COMPOSITION.

[4] J. Groenestijn. Microfluidic platform for Coriolis-based sensor and actuator systems section 7.3.

[5] Electronic notes : Dielectric constant and Relative permittivity. https://www.electronics-notes.com/articles/basic_concepts/capacitance/dielectric-constant-relative-permittivity.php

[6] Keysight Technologies : Basics of measuring the Dielectric Properties of Materials page 20. http://literature.cdn.keysight.com/litweb/pdf/5989-2589EN.pdf

[7] B.E. Poling, J.M.Prausnitz, J.S.Rowlinson. Liquid : state of matter https://www.britannica.com/science/liquid-state-of-matter#ref506795

[8] Capacitance:Unit and Formula. https://study.com/academy/lesson/capacitance-units-formula.html

[9] Hanasi et al. Study of Capacitance in Electrostatic Comb-Drive Actuators. https://uk.comsol.com/paper/download/295221/hanasi_paper.pdf

[10] Introduction to COMSOL Multiphysics 5.3a. https://cdn.comsol.com/documentation/5.3.1.348/IntroductionToCOMSOLMultiphysics.pdf

[11] AZO materials : Silicon Nitride Properties and Application https://www.azom.com/properties.aspx?ArticleID=53

[12] Engineering toolbox : Permittivities of some fluids. https://www.engineeringtoolbox.com/relative-permittivity-d_1660.html